

Finite temperature dynamics in a polarized sub-Ohmic heat bath: a hierarchical equations of motion-tensor train study

Hideaki Takahashi,¹ Raffaele Borrelli,¹ Maxim F. Gelin,² and Lipeng Chen³

¹*DISAFA, University of Torino, Grugliasco, Italy*

²*School of Science, Hangzhou Dianzi University, Hangzhou 310018, China*

³*Zhejiang Laboratory, Hangzhou 311100, China*

(*Electronic mail: chenlp@zhejianglab.com)

(*Electronic mail: maxim@hdu.edu.cn)

(*Electronic mail: raffaele.borrelli@unito.it)

Dynamics of the sub-Ohmic spin-boson model under polarized initial conditions at finite temperature is investigated by employing both analytical tools and the numerically accurate hierarchical equations of motion-tensor train method. By analyzing the features of nonequilibrium dynamics, we discovered a bifurcation phenomenon which separates two regimes of the dynamics. It is found that before the bifurcation time, increasing temperature slows down the population dynamics, while the opposite effect occurs after the bifurcation time. The dynamics is highly sensitive to both initial preparation of the bath and thermal effects.

I. INTRODUCTION

Understanding microscopic mechanisms responsible for relaxation and decoherence of quantum systems coupled to their environments is the central task of open quantum systems.^{1,2} Due to the intricate interplay between electronic and vibrational degrees of freedom (DOFs), accurate simulation of the dynamics of dissipative systems is a formidable challenge. A common way for the evaluation of the dynamics of open quantum systems is based on quantum master equations (QMEs). The key ingredients of this methodology are tracing out environmental DOFs and obtaining equations of motion for the reduced (system) density matrix.³ In many scenarios, however, the system-environment coupling is not weak, and dynamic timescales of the system and the environment are comparable. As a result, traditional QMEs based on the Markovian and/or weak system-bath coupling approximations are no longer valid.^{4,5} To capture the intrinsic non-perturbative and non-Markovian effects, several advanced numerically accurate methods and simulation protocols have been developed. The quadiabatic propagator path integral (QUAPI),^{6,7} the hierarchy equations of motion (HEOM)^{8,9} and the path integral Monte Carlo (PIMC)^{10,11} are typical examples of numerically exact QME approaches to the propagation of the reduced density matrix.

Alternative methodology is based on the discretization of the bath DOFs and the numerical evaluation of the combined system-bath time dependent Schrödinger equation. Several formally exact wave function methods are available for the simulation of the dynamics at zero temperature. They include the multiconfiguration time-dependent Hartree (MCTDH) method¹² and its multilayer variant (ML-MCTDH),^{13–15} the time-dependent density matrix renormalization group (TD-DMRG),^{16–18} the time-evolving block-decimation (TEBD) method,^{19–21} the multiple Davydov Ansatz (mDA),^{22,23} the multi-configuration Ehrenfest,^{24–26} and various variants of the matrix-product-state (MPS) methods.^{27–31} A promising technique to simulate finite-temperature dynamics with wave-function methods is based on the so-called thermo-field

dynamics-tensor train (TFD-TT) approach.³²

The spin-boson model (SBM), which describes two-level system coupled to the bath of harmonic oscillators, has established itself as perhaps one of the most widely studied models which facilitated understanding of relaxation and decoherence processes in open quantum systems. Despite its simple formulation, the SBM has attracted widespread attention over past years due to the rich physics it exhibits. It is thus not surprising that the dynamics of the SBM was simulated with virtually all aforementioned methods.^{33–43} Variational quantum algorithms were also employed to calculate the dynamics of the SBM.⁴⁴

In the context of the present study, we wish to highlight several key results obtained on the dynamics of the SBM. For the Ohmic bath with spectral density $J(\omega) \sim \omega^s$ and spectral exponent $s = 1$, increasing system-bath coupling turns the system dynamics incoherent and causes delocalized-localized phase transition at zero temperature.^{1,2} The sub-Ohmic bath with spectral exponent $s < 1$ is characterized by the pronounced effect of low-frequency modes, which leads to strongly non-Markovian dynamics even for relatively weak system-bath interactions. Numerical simulations based on the ML-MCTDH method have shown that the dynamics of the SBM changes from the weakly damped coherent motion to localization when the system-bath coupling increases.^{45,46} Both QUAPI and MPS simulations have revealed that the initial preparation of the bath has considerable influence on the dynamics of the sub-Ohmic SBM.^{47,48} Using the PIMC method, it was further found that, under the polarized bath initial condition, the oscillatory dynamics persists irrespective of the system-bath coupling strength for $0 < s < 1/2$.^{49,50} For the factorized bath initial condition, the zero-temperature dynamic phase diagram containing coherent, pseudocoherent and incoherent phases was obtained by using the numerical technique based on the time-evolving matrix product operator.⁵¹ In a recent work, the zero-temperature dynamic phase diagrams of the sub-Ohmic SBM were identified under various bath initial conditions by employing the mDA.⁵² The TFD-TT methodology was harnessed for studying finite-

temperature effects on the dynamics of the SBM.⁵³

In this paper, we delve into the still unexplored area of the dynamics of the sub-Ohmic SBM. By employing the HEOM in the twin-space (TS) representation and TT format, we perform dynamic simulations of the sub-Ohmic SBM under the polarized bath initial condition. We demonstrate that the HEOM-TSTT method is capable of accurately evaluating long-time dynamics of the sub-Ohmic SBM at any temperature. The rest of the paper is organized as follows. In Sec. II, we introduce the SBM and the HEOM-TSTT method. In Sec. III, we discuss temperature effects on the dynamics of the sub-Ohmic SBM. Conclusions are drawn in Sec. IV.

Throughout this paper, we set the reduced Planck constant $\hbar = 1$ and the Boltzmann constant $k_B = 1$, as well as employ dimensionless variables.

II. THEORY

A. Hamiltonian

The Hamiltonian of the SBM can be written as

$$\hat{H} = \hat{H}_S + \hat{H}_B + \hat{H}_{SB} \quad (1)$$

where

$$\begin{aligned} \hat{H}_S &= -\frac{1}{2}\Delta\hat{\sigma}_x + \frac{1}{2}\varepsilon\hat{\sigma}_z \\ \hat{H}_B &= \sum_k \omega_k \hat{b}_k^\dagger \hat{b}_k \\ \hat{H}_{SB} &= \frac{1}{2}\hat{\sigma}_z \sum_k \lambda_k (\hat{b}_k^\dagger + \hat{b}_k) \end{aligned} \quad (2)$$

For the spin system, $\hat{\sigma}_x$ and $\hat{\sigma}_z$ are Pauli matrices, and ε and Δ are the spin bias and the bare tunneling constant. For the bath, \hat{b}_k^\dagger (\hat{b}_k) is the creation (annihilation) operator of the k th bosonic mode with frequency ω_k . The system-bath interaction follows a bilinear form with λ_k being the coupling strength. The bath is characterized by the spectral density function

$$J(\omega) = \sum_k |\lambda_k|^2 \delta(\omega - \omega_k) = 2\alpha\omega_c^{1-s} \omega^s e^{-\omega/\omega_c}. \quad (3)$$

Here, α is the Kondo parameter specifying the dimensionless coupling strength, ω_c is the cutoff frequency, and s is the spectral exponent. The bath is categorized as sub-Ohmic ($0 < s < 1$), Ohmic ($s = 1$) and super-Ohmic ($s > 1$). In this paper, we limit our investigation to the sub-Ohmic bath which is characterized by strong non-Markovian effects induced by low frequency bath modes.

B. Shifted initial condition

Dynamics of the sub-Ohmic SBM is sensitive to the initial preparation of the bath.^{47,49,54} Two kinds of bath initial conditions are usually considered, the so-called factorized initial condition and the shifted (polarized) initial condition. For the

factorized initial condition, the spin system is in thermal equilibrium with the bath at temperature T and at the initial time $t = 0$, i.e.,

$$\hat{\rho}(t=0) = \hat{\rho}_S(t=0) \otimes \hat{\rho}_B \quad (4)$$

Here, $\hat{\rho}(t=0)$ and $\hat{\rho}_S(t=0)$ are initial total and system density matrices, respectively, and

$$\hat{\rho}_B = e^{-\beta\hat{H}_B} / \text{Tr}\{e^{-\beta\hat{H}_B}\} \quad (5)$$

is the equilibrium (Boltzmann) bath distribution at the inverse temperature $\beta = 1/T$.

For the shifted (polarized) initial condition, one prepares the spin long time before the bath can thermalize to the shifted spin, i.e.,

$$\hat{\rho}(t=0) = \hat{\rho}_S(t=0) \otimes \hat{\rho}_{B\mu} \quad (6)$$

with

$$\hat{\rho}_{B\mu} = e^{-\beta(\hat{H}_B + \hat{H}_{SB}|\hat{\sigma}_z=\mu)} / \text{Tr}\{e^{-\beta(\hat{H}_B + \hat{H}_{SB}|\hat{\sigma}_z=\mu)}\} \quad (7)$$

where μ is a parameter characterizing the degree of the bath polarization. In particular, $\mu = 0$ corresponds to the factorized initial condition of Eq. (4). In the present work, we explore the impact of the shifted initial condition of Eq. (6) on the dynamics of the sub-Ohmic SBM at finite temperature.

C. Transformed Hamiltonian

The dynamics of the SBM under factorized and shifted initial conditions are closely related. To demonstrate that, we formulate the following statement,

Theorem. The Liouville-von Neumann (LvN) equation

$$\partial_t \hat{\rho}(t) = -i[\hat{H}, \hat{\rho}(t)] \quad (8)$$

governed by the SBM Hamiltonian \hat{H} under the shifted initial condition of Eq. (6) is equivalent to the LvN equation

$$\partial_t \hat{\rho}(t) = -i[\hat{H}_\mu, \hat{\rho}(t)] \quad (9)$$

governed by the modified SBM Hamiltonian \hat{H}_μ under the factorized initial condition of Eq. (4). Here the modified SBM Hamiltonian

$$\hat{H}_\mu = \hat{H}_S^\mu + \hat{H}_B + \hat{H}_{SB}^\mu \quad (10)$$

has the same structure as the original SBM Hamiltonian \hat{H} , but its parameters become μ -dependent:

$$\hat{H}_S^\mu = -\frac{\Delta}{2}\hat{\sigma}_x + \frac{\varepsilon - \mu E_R}{2}\hat{\sigma}_z, \quad (11)$$

$$\hat{H}_{SB}^\mu = \frac{\hat{\sigma}_z - \mu}{2} \sum_k \lambda_k (\hat{b}_k^\dagger + \hat{b}_k). \quad (12)$$

Here

$$E_R = \int_0^\infty \frac{J(\omega)}{\omega} d\omega = 2\alpha\omega_c \Gamma(s) \quad (13)$$

is the reorganization energy and $\Gamma(s)$ denotes the Gamma function.

Proof. We can rewrite the Hamiltonian

$$\hat{H}_{B\mu} = \hat{H}_B + \hat{H}_{SB}|_{\hat{\sigma}_z=\mu}$$

as

$$\begin{aligned} \hat{H}_{B\mu} &= \sum_k \omega_k \hat{b}_k^\dagger \hat{b}_k + \frac{\mu}{2} \sum_k \lambda_k (\hat{b}_k^\dagger + \hat{b}_k) \\ &= \sum_k \omega_k (\hat{b}_k^\dagger + \mu \frac{\lambda_k}{2\omega_k}) (\hat{b}_k + \mu \frac{\lambda_k}{2\omega_k}) - \mu^2 \sum_k \frac{\lambda_k^2}{4\omega_k} \\ &= \hat{H}_{B\mu}^R - \frac{\mu^2}{4} E_R \end{aligned} \quad (14)$$

where

$$\hat{H}_{B\mu}^R = \sum_k \omega_k (\hat{b}_k^\dagger + \mu \frac{\lambda_k}{2\omega_k}) (\hat{b}_k + \mu \frac{\lambda_k}{2\omega_k}).$$

Obviously, the Boltzmann distributions corresponding to $\hat{H}_{B\mu}$ and $\hat{H}_{B\mu}^R$ are identical,

$$\hat{\rho}_{B\mu} = \frac{e^{-\beta \hat{H}_{B\mu}}}{\text{Tr}\{e^{-\beta \hat{H}_{B\mu}}\}} = \hat{\rho}_{B\mu}^R = \frac{e^{-\beta \hat{H}_{B\mu}^R}}{\text{Tr}\{e^{-\beta \hat{H}_{B\mu}^R}\}}. \quad (15)$$

Let us now introduce the new shifted creation (annihilation) operator for the k th bosonic mode

$$\hat{c}_k^\dagger = \hat{b}_k^\dagger + \mu \frac{\lambda_k}{2\omega_k}, \quad \hat{c}_k = \hat{b}_k + \mu \frac{\lambda_k}{2\omega_k} \quad (16)$$

(the transformation is equivalent to the polaron transformation² of the original Hamiltonian). In the representation of the new operators, the Boltzmann distribution $\hat{\rho}_{B\mu}(\hat{b}_k^\dagger, \hat{b}_k)$ corresponds to the factorized initial condition, i.e., $\hat{\rho}_{B\mu}(\hat{b}_k^\dagger, \hat{b}_k) \Leftrightarrow \hat{\rho}_B(\hat{c}_k^\dagger, \hat{c}_k)$. In the new representation, the original Hamiltonian \hat{H} has the form

$$\begin{aligned} \hat{H} &= -\frac{\Delta}{2} \hat{\sigma}_x + \frac{\varepsilon}{2} \hat{\sigma}_z + \sum_k \omega_k \hat{b}_k^\dagger \hat{b}_k + \frac{\hat{\sigma}_z}{2} \sum_k \lambda_k (\hat{b}_k^\dagger + \hat{b}_k) \\ &= -\frac{\Delta}{2} \hat{\sigma}_x + \frac{\varepsilon}{2} \hat{\sigma}_z + \sum_k \omega_k (\hat{c}_k^\dagger - \mu \frac{\lambda_k}{2\omega_k}) (\hat{c}_k - \mu \frac{\lambda_k}{2\omega_k}) \\ &\quad + \frac{\hat{\sigma}_z}{2} \sum_k \lambda_k (\hat{c}_k^\dagger - \mu \frac{\lambda_k}{2\omega_k} + \hat{c}_k - \mu \frac{\lambda_k}{2\omega_k}) \\ &= -\frac{\Delta}{2} \hat{\sigma}_x + \frac{\varepsilon - \mu E_R}{2} \hat{\sigma}_z + \sum_k \omega_k \hat{c}_k^\dagger \hat{c}_k \\ &\quad + \frac{\hat{\sigma}_z - \mu}{2} \sum_k \lambda_k (\hat{c}_k^\dagger + \hat{c}_k) + \frac{\mu^2}{4} E_R \end{aligned} \quad (17)$$

The above expression yields the Hamiltonian of Eq. (10), in which we dropped the constant term of $\mu^2 E_R/4$ since it does not affect any dynamics.

Mapping of the shifted SBM to the factorized one facilitates numerical simulations. It demonstrates that the dynamics of the SBM under shifted initial conditions can be obtained

with any method developed for the standard factorized initial conditions. One just has to use the modified Hamiltonian \hat{H}_μ instead of \hat{H} . This is employed in the present work for the construction of the HEOM-TSTT integrator for the SBM under shifted initial conditions.

D. HEOM in twin space

In the following we will make use of the TS formulation of the LvN equation. The reader is referred to the original papers for the comprehensive discussion on the topic,^{55–58} but for the subsequent presentation it is enough to realize that the LvN equation (9) in the TS representation takes the form

$$\partial_t |\rho(t)\rangle = -i(\hat{H}_\mu - \tilde{\hat{H}}_\mu) |\rho(t)\rangle. \quad (18)$$

Here $\tilde{\hat{H}}_\mu$ is a copy of the Hamiltonian \hat{H}_μ acting on the so-called *tilde* Hilbert space, which is an exact copy of the original Hilbert space where the system dynamical variables are defined. Eq. (18) is the departing point for the derivation of the HEOM-TSTT, as recently proposed by Borrelli.⁵⁵ Below we briefly sketch the main steps of the derivation, and further details can be found in Refs.^{55,59,60}

First of all we represent Eq. (18) in the interaction representation. Then we notice that the time evolution of the reduced density matrix governed by the modified Hamiltonian of Eq. (10) can be evaluated as^{61,62}

$$|\rho_S(t)\rangle_I = T_+ \exp\left(-\int_0^t \hat{K}_I^{(2)}(s) ds\right) |\rho(0)\rangle_I \quad (19)$$

where

$$\hat{K}_I^{(2)}(s) = \int_0^s d\tau \langle \hat{H}_{SB}^\mu(s) \hat{H}_{SB}^\mu(\tau) \rangle, \quad (20)$$

T_+ is the time-ordering operator, and the subscript I indicates the interaction representation. Starting from the modified Hamiltonian of Eq. (10), after some easy manipulations, it is possible to write the second order cumulant in the form

$$\begin{aligned} \hat{K}_I^{(2)}(t) &= \sum_k [S(t) - \tilde{S}(t)] [C_R(t-s)(S(s) - \tilde{S}(s)) \\ &\quad + C_I(t-s)(S(s) + \tilde{S}(s))] \end{aligned} \quad (21)$$

where $C_R(t) = (C(t) + C^*(t))/2$, $C_I(t) = (C(t) - C^*(t))/2$ are the symmetric and antisymmetric part of the bath correlation function (BCF) $C(t)$, respectively, $S = (\sigma_z - \mu)/2$ is the system operator, and \tilde{S} is the *tilde* counterparts.

Following the standard theory of HEOM we assume that both BCF components can be decomposed into a sum of exponential functions

$$C_X(t-s) = \sum_{j=1}^{J_X} c_{Xj} e^{-\gamma_{Xj}|t-s|} \quad (22)$$

where c_{Xj} and γ_{Xj} with $X = R, I$ are complex numbers, and J_X is the number of terms for the expansion of the X component of $C(t)$. This decomposition is crucial for disentangling

the time-ordering in the time-evolution of the reduced density matrix. The set of coefficients and exponents can be obtained using a variety of techniques whose choice depends on the type of the spectral density.^{63–65}

The key to the derivation of the HEOM-TSTT is the definition of the so-called auxiliary density vectors (ADV)⁶⁶

$$\begin{aligned} |\rho_S^{\mathbf{mn}}(t)\rangle &= T_+ \prod_j (m_j! c_{Rj}^{m_j})^{-1/2} \\ &\left(i \int_0^t ds e^{-\gamma_{Rj}|t-s|} (S_{Rj}(s) - \tilde{S}_{Rj}(s)) \right)^{m_j} \\ &\times \prod_j (n_j! (c_{Ij})^{n_j})^{-1/2} \left(i \int_0^t ds e^{-\gamma_{Ij}^*|t-s|} (S_{Ij}(s) + \tilde{S}_{Ij}(s)) \right)^{n_j} \\ &\times \exp\left(-\int_0^t \hat{K}_I^{(2)}(s) ds\right) |\rho_S(0)\rangle \end{aligned} \quad (23)$$

where $|\rho_S(0)\rangle$ is the reduced density matrix of the system, $\mathbf{m} = \{m_j\}$, $\mathbf{n} = \{n_j\}$ are two sets of non-negative integers and

$$S_{Xj} = \sqrt{c_{Xj}} S, \quad X = R, I. \quad (24)$$

In the above formalism we have $J_R + J_I$ auxiliary spectral density vectors. It is readily verified that the vector $|\rho_S(t)\rangle_I$, describing the physical state of our system, corresponds to the auxiliary state vector having all indices $(m_j, n_j) = 0$, i.e. $|\rho_S(t)\rangle_I = |\rho_S^0(t)\rangle$. The above definition takes into account the scaling originally proposed by Shi and coworkers which improves the numerical stability of the final system of equations.⁶⁷

The HEOM are readily derived upon repeated differentiation of $|\rho_S^{\mathbf{mn}}\rangle$ with respect to time and then moving to the Schrödinger representation. The final result can be written in the form

$$\begin{aligned} \frac{\partial}{\partial t} |\rho_S^{\mathbf{mn}}\rangle &= -(i\hat{H}_S^\mu + \sum_j m_j \gamma_{Rj} + \sum_j n_j \gamma_{Ij}) |\rho_S^{\mathbf{mn}}\rangle \\ &- i \sum_j \sqrt{m_j + 1} (S_{Rj} - \tilde{S}_{Rj}) (|\rho_S^{\mathbf{m}+1_j \mathbf{n}}\rangle \\ &- i \sum_j \sqrt{m_j} (S_{Rj} - \tilde{S}_{Rj}) |\rho_S^{\mathbf{m}-1_j \mathbf{n}}\rangle \\ &- i \sum_j \sqrt{n_j + 1} (S_{Ij} - \tilde{S}_{Ij}) |\rho_S^{\mathbf{m} \mathbf{n}+1_j}\rangle \\ &+ \sum_j \sqrt{n_j} (S_{Ij} + \tilde{S}_{Ij}) |\rho_S^{\mathbf{m} \mathbf{n}-1_j}\rangle. \end{aligned} \quad (25)$$

The HEOM consist of an infinite set of first-order ordinary differential equations. Fortunately, it is possible to devise very efficient truncation schemes which allow us to obtain highly accurate results for the reduced system dynamics. The reader is referred to the original papers for the description of the optimal truncation scheme.^{68,69} In the above derivation we have not considered low-temperature corrections which can be included straightforwardly from a direct application of the original approach suggested by Ishizaki and Tanimura.⁶⁹

The HEOM-TSTT equations resemble their HEOM counterparts in the standard density matrix formalism (see, for example, Ref.⁶²). However, in the present case, commutators

and anti-commutators are replaced by differences and sums of the physical and tilde operators. As we shall see in the next section, this has several benefits for the numerical implementation of the HEOM solver.

To further simplify the HEOM-TSTT structure, we introduce two sets of boson-like creation-annihilation operators b_{Rj}^+, b_{Ij}^- and $\tilde{b}_{Rj}^+, \tilde{b}_{Ij}^-$ acting respectively on the set of state vectors $|\mathbf{m}\rangle = |m_0 \dots m_{J_R}\rangle$, and $|\mathbf{n}\rangle = |n_0 \dots n_{J_I}\rangle$,

$$b_{Rj}^+ |\mathbf{m}\rangle = \sqrt{(m_j + 1)} |\mathbf{m} + 1_j\rangle, \quad b_{Rj}^- |\mathbf{m}\rangle = \sqrt{m_j} |\mathbf{m} - 1_j\rangle \quad (26)$$

$$\tilde{b}_{Ij}^+ |\mathbf{n}\rangle = \sqrt{(n_j + 1)} |\mathbf{n} + 1_j\rangle, \quad \tilde{b}_{Ij}^- |\mathbf{n}\rangle = \sqrt{n_j} |\mathbf{n} - 1_j\rangle \quad (27)$$

we then define the vector

$$|\rho(t)\rangle = \sum_{\mathbf{mn}} |\rho_S^{\mathbf{mn}}(t)\rangle |\mathbf{mn}\rangle \quad (28)$$

and rewrite the HEOM-TSTT in the compact form

$$\begin{aligned} \frac{\partial}{\partial t} |\rho\rangle &= \left[-i\hat{H}_S^\mu - \sum_{j, X=R, I} \gamma_{Xj} b_{Xj}^+ b_{Xj}^- \right. \\ &- i \sum_{j, X=R, I} (S_{Xj} - \tilde{S}_{Xj}) b_{Xj}^- \\ &\left. - i \sum_j (S_{Rj} - \tilde{S}_{Rj}) b_{Rj}^+ + \sum_j (S_{Ij} + \tilde{S}_{Ij}) \tilde{b}_{Ij}^+ \right] |\rho\rangle, \end{aligned} \quad (29)$$

with the initial condition given by $|\rho(0)\rangle = |\rho_S(0)\rangle |\mathbf{0}\rangle$.

Finally, we mention that the TS formulation of HEOM has been recently extended to treat the interaction of molecules with fermionic baths at finite temperature. The approach is very similar to the one introduced above, and the reader is referred to the original papers for mathematical details.^{70,71}

E. TT representation of auxiliary density vectors

The size of the set of equations (29) increases exponentially with the number of expansion terms of the spectral density and, besides, the equations are known to be rather unstable.⁷² The numerical solution is usually tackled by truncating the hierarchy in such a way that all ADVs with $\sum_k n_{ik} > D$ are set to zero, where D is a prescribed integer. Typical values of D range from 4 to 10, depending on the degree of non-Markovianity of the bath. While this truncation scheme is rather effective and can significantly reduce the computational burden of the numerical solution of HEOM,⁷³ it cannot solve the inherent exponential scaling of the number of equations. Only very recently, Shi⁶⁰ and later Borrelli⁵⁵ have shown that it is possible to use TT techniques to overcome this problem and significantly expand the range of applications of the HEOM methodology.

In the following we sketch the basic principles of the TT decomposition,^{74–81} and show how it can be applied to solve the HEOM-TSTT equation (29).

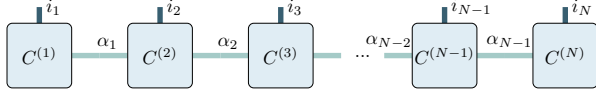


Figure 1. Graphical representation of a TT. Each square node represents a core of the TT, and each vertical line represents an index i_k of the tensor. Connecting lines represent the contractions over the indices α_k .

Let us first recall the basic principles of the TT decomposition by considering a generic expression of a state of a N -dimensional quantum system at time t in the form

$$|\rho(t)\rangle = \sum_{i_1, i_2, \dots, i_N} C_t(i_1, \dots, i_N) |i_1\rangle \otimes |i_2\rangle \cdots |i_N\rangle. \quad (30)$$

where $|i_k\rangle$ labels the basis states of the k th dynamical variable, and the elements $C_t(i_1, \dots, i_N)$ are complex numbers labeled by N indices. If we truncate the summation of each index i_k to a maximum value p_k , the elements $C_t(i_1, \dots, i_N)$ represent a tensor of order N . Evaluation of the summation in Eq. (30) requires computation (and storage) of p^N terms with p being the average size of the one-dimensional basis set, which becomes prohibitive for large N . Using the TT format, the tensor C_t is approximated as

$$C_t(i_1, \dots, i_N) \approx C^{(1)}(i_1)C^{(2)}(i_2) \cdots C^{(N)}(i_N) \quad (31)$$

where $C^{(k)}(i_k)$ is a $r_{k-1} \times r_k$ complex matrix, $k = 1, \dots, N$ (for the moment, let us drop the time variable for simplicity). In the explicit index notation

$$C_t(i_1, \dots, i_N) \approx \sum_{\alpha_0, \dots, \alpha_N=1}^{r_0, \dots, r_N} C_{\alpha_0, \alpha_1}^{(1)}(i_1) C_{\alpha_1, \alpha_2}^{(2)}(i_2) \cdots C_{\alpha_{N-1}, \alpha_N}^{(N)}(i_N). \quad (32)$$

The trailing indices α_0 and α_N are introduced for uniformity of notation, but to render the right-hand side scalar, we always set $r_0 = r_N = 1$. The factors $C^{(k)}$ are three-dimensional arrays, called *cores* of the TT decomposition. The dimensions r_k are called TT ranks. The TT decomposition (31) is also known under the name of the MPS.^{82,83} In the MPS language, the TT ranks are referred to as *bond dimensions*. Using the TT decomposition of Eq. (31) it is possible, at least in principle, to overcome most of the difficulties caused by the dimension of the problem. Indeed, the wave function is entirely defined by N arrays of dimensions $r_{k-1} \times p_k \times r_k$ thus requiring a storage dimension of the order Npr^2 . The TT-decomposition is visualized in Fig. 1.

Turning now to the representation of the ADV of Eq. (28) in the TT format we let d be the number of DOFs of the Hamiltonian operator \hat{H}_S^μ , and assume that the dissipative environment is described using M uncorrelated spectral densities $J_k(\omega)$ each expanded into J Matstubara terms. Hence, the ADV can be considered as a tensor with $N = 2(d + JM)$ indices. Therefore, in Eq. (32) the first $2d$ indices label the physical and tilde DOFs of the system, and the remaining $2JM$ indices label the bath operators.

F. Fitting of the sub-Ohmic spectral density

The expansion of the symmetric ($X = R$) and antisymmetric ($X = I$) part of the BCF $C_X(t)$ using equation (22) is a complex task that strongly affects the accuracy of the solution, for which many procedures have been developed.⁹ In this work we have used the so-called ESPRIT fitting methodology,^{84–86} which is a direct time-domain fitting procedure. For a given BCF component $C_X(t)$ with $X = R, I$, we consider the vector $\mathbf{f} = (f_0, f_1, \dots, f_{2N-2})^T$ where each element $f_j = C_X(t_j)$ is sampled on an equispaced grid $t_j = hj$, ($h = \frac{t_{\max}}{2N-2}$, $j = 0, 1, \dots, 2N-2$) and $N > M$. Here we assume that f_j can be expressed as

$$f_j = \sum_{k=1}^M c_k e^{-a_k h j} = \sum_{k=1}^M c_k z_k^j, \quad (33)$$

where $c_k \in \mathbb{C}$ and $z_k = e^{-a_k h} \in \mathbb{D}$, and the symbol \mathbb{D} denotes the complex unit disk without zero. Accordingly, the problem is reduced to a problem of finding complex weights $\mathbf{c} = (c_1, \dots, c_M)^T$ and complex nodes $\mathbf{z} = (z_1, \dots, z_M)^T$ with a minimal number of terms M for a given accuracy ε , which is written as

$$\left\| f_j - \sum_{k=1}^M c_k z_k^j \right\| < \varepsilon \quad (34)$$

for all $j = 0, \dots, 2N-2$. ESPRIT algorithm relies on the rank reduction of the Hankel matrix $H_{N,N} = (f_{k+l})_{k,l=0}^{N-1, N-1}$, which has f_j as entries, and the overdetermined least-squares Vandermonde system. While ESPRIT is similar to Prony's method^{87,88} in principle, it offers greater stability and improved accuracy. In this study, we refer to Algorithm 1 in Ref. 84 and use the routine DQAG from the QUADPACK library with an accuracy of $\varepsilon_{\text{DQAG}} = 10^{-12}$ to obtain highly accurate data of \mathbf{f} through the quantum fluctuation-dissipation theorem.

III. RESULTS AND DISCUSSION

In this section, we systematically study the spin dynamics $P_z(t)$ for different values of the system-bath coupling α and the bath exponent s at various temperatures T . We begin with analytical results, discussing the short-time expansion of $P_z(t)$ in Sec. III A. Then we present results of the HEOM-TSTT simulations in Sec. III B. In all HEOM-TSTT calculations, we set $\Delta = 0.1$ and $\varepsilon = 0$ as well as consider the strongly polarized initial condition ($\mu = 1$). The cutoff frequency of the bath is chosen as the unit of energy, $\omega_c = 1$.

A. Short-time expansion of $P_z(t)$

The simulation of the dynamics of the SBM at zero temperature with the spectral density of Eq. (3) revealed the following rule-of-thumb principle. The time evolution of $P_z(t)$

calculated for a series of coupling strengths α or bath exponents s at zero temperature do not intersect each other up to quite long times t (see, e.g., Refs.^{46,51,52}). This observation hints that the inspection of the short-time behavior of $P_z(t)$ can be useful for the analyses of $P_z(t)$.

The transformation of Sec. II C can be conveniently used for performing the Taylor-series expansion of $P_z(t)$, because the evaluation of necessary expectation values with the equilibrium Boltzmann distribution of Eq. (5) can be done straightforwardly with standard methods. We thus need to evaluate

$$P_z(t) = \text{Tr}\{\hat{\sigma}_z \hat{\rho}(t)\} = \sum_{a=0}^{\infty} \text{Tr}\{\hat{\sigma}_z \hat{\rho}_a\} \frac{t^a}{a!},$$

where

$$\hat{\rho}_0 = |\uparrow\rangle\langle\uparrow| \hat{\rho}_B, \quad \hat{\rho}_{a+1} = -i[\hat{H}_\mu, \hat{\rho}_a].$$

A tedious but straightforward calculation yields the following result,

$$P_z(t) = 1 - 2\Delta^2 t^2 + \Delta^2 (\Omega_\mu^2 + Y) t^4 / 6 + O(t^6). \quad (35)$$

Here

$$\Omega_\mu = \sqrt{(\varepsilon + \mu E_R)^2 + 4\Delta^2} \quad (36)$$

is the μ -renormalized Rabi frequency, and

$$Y = \int d\omega J(\omega) \coth\left(\frac{\omega}{2T}\right). \quad (37)$$

According to Eq. (13), the reorganization energy E_R increases with α , decreases with s , and is temperature-independent. As a result, the Rabi-frequency Ω_μ is also temperature-independent, but depends significantly on the system preparation (parameter μ), as well as increases with α and decreases with s . For the bath spectral density of Eq. (3), Y cannot be evaluated in the closed form for finite T . It is crucial though that it is strictly positive, increases with temperature (it can immediately be verified that $dY/dT > 0$) as well as grows with the coupling strength α . As a function of the spectral exponent s , Y is U-shaped, exhibiting a T -dependent minimum.

The expansion of Eq. (35) contains only even powers of time owing to the time reversibility of the Hamiltonian dynamics. The term $\sim t^2$ is negative and is exclusively determined by the spin system, that is, by the tunneling Δ . This term describes the short-time dynamics and specifies the so-called Zeno time $\tau_Z = \Delta^{-1}/\sqrt{2}$, meaning that the initial depopulation can be approximated as

$$P_z(t) \approx \exp[-(t/\tau_Z)^2] + O(t^4)$$

(see, e.g. Refs.^{89,90}). The term $\sim t^4$ is strictly positive and depends on the bath parameters and temperature. On the basis of the scaling properties of E_R and Y established above, we can therefore conclude that $P_z(t)$ increases with α and T . In Sec. III B, we will explore how these short-time results can be used to help understanding global $P_z(t)$ dynamics at finite temperature and polarized initial conditions.

Note that Y can be analytically evaluated at zero temperature. The result reads as $Y = 2\alpha\omega_c^2\Gamma(s+1)$. It is known that $\Gamma(s)$ decreases with s for $0 < s < 1.462$, reaches its minimum at $\Gamma(1.462) = 0.886$ and then increases for $s > 1.462$. Taking into account that $E_R \sim \Gamma(s)$ according to Eq. (13), $P_z(t)$ decreases with s for $0 < s < 0.462$ and increases for $s > 1.462$. The behavior for $0.462 < s < 1.462$ is determined by the interplay of Ω_μ^2 (decreases with s) and Y (increases with s), which probably explains why the value of $s \approx 0.46$ is the bifurcation point in the $s - \alpha$ phase diagrams.^{51,52}

Eq. (35) can be used to anticipate the microscopically justified fitting functions for $P_z(t)$. One of the possible expression reads

$$P_z(t) = 1 - 4 \frac{\Delta^2}{\Omega_\mu^2(T)} (1 - \cos(\Omega_\mu(T)t)) + O(t^6) \quad (38)$$

where

$$\Omega_\mu(T) = \sqrt{\Omega_\mu^2 + Y} \quad (39)$$

is the effective temperature-dependent Rabi frequency. This formula is inspired by the following observation, for bath-free SBM ($E_R = Y = 0$) we recover the standard Rabi formula. Since Y increases with temperature, Eq. (39) predicts that temperature increases the effective Rabi frequency $\Omega_\mu(T)$ and therefore shortens the period of Rabi oscillations.

B. HEOM-TSTT simulations of $P_z(t)$

Fig. 2 displays populations $P_z(t)$ for the sub-Ohmic bath with exponent $s = 0.25$ at different system-bath couplings α and temperatures T . At $T = 0$, the oscillation frequency of $P_z(t)$ increases with increasing system-bath coupling (cf. Eq. (39)) and the oscillatory behavior survives for larger couplings α , in agreement with previous results.^{46,47,49,52} With the increase of coupling α , $P_z(t)$ increase (that is, lie above each other) up to $t \approx 45$, in accordance with the explanations of Sec. III A. Increasing temperature acts against localization, inducing and/or fastening decay and quenching oscillations in $P_z(t)$. The bath-induced decay becomes especially pronounced in the regime of large couplings α . Qualitatively, these dynamical behaviors of the SBM prepared under the shifted initial condition of Eq. (6) match those of the SBM prepared under the factorized initial condition of Eq. (4), but specific characteristics (e.g. periods of oscillations or decay rates) are significantly μ -dependent (cf. Refs.^{49,50,52}).

Fig. 3 shows $P_z(t)$ for the sub-Ohmic bath with $s = 0.5$. All qualitative trends for the dynamical behavior of $P_z(t)$ induced by changing the system-bath coupling α and temperature T remain the same. However, $P_z(t)$ in Fig. 3 do not exhibit localization for $t \leq 100$ at $T = 0$ and relatively strong coupling. In addition, the bath with $s = 0.5$ is much less efficient than the bath with $s = 0.25$ in quenching Rabi oscillations in the weak-coupling limit ($\alpha = 0.01$). Indeed, the black curves in Fig. 3 exhibit almost full recurrence at $t \approx 65$ at zero temperature, and show pronounced underdamped oscillations at

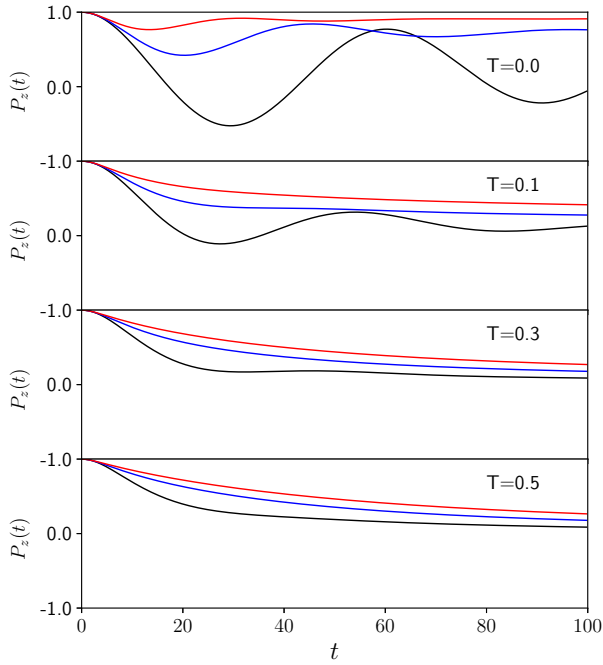


Figure 2. Spin dynamics $P_z(t)$ for the sub-Ohmic bath with $s = 0.25$ and $\alpha = 0.01, 0.03, 0.05$ (black, blue, and red lines, respectively) for several T indicated in the panels.

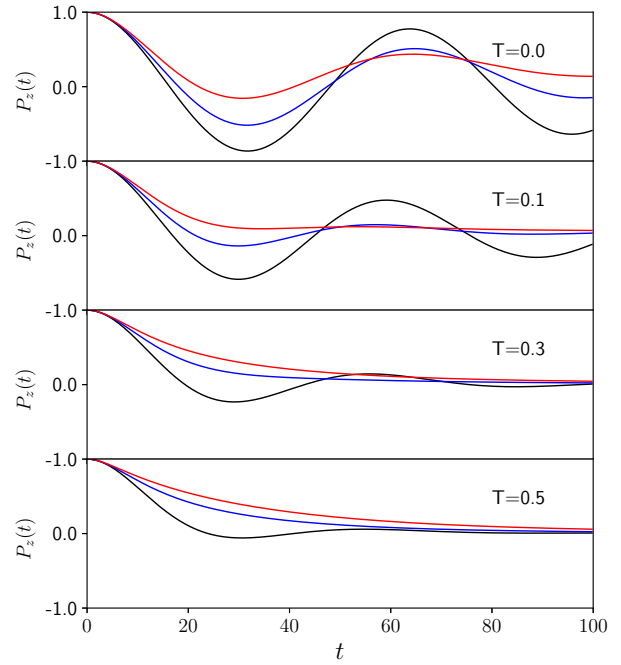


Figure 3. Same as in Fig. 2 but for $s = 0.5$.

finite temperatures. The aforementioned enhancement of oscillations is in full agreement with the calculations of Ref.⁵² at $T = 0$.

Fig. 4 is the counterpart of Figs. 2 and 3 for $s = 0.75$. The general trends in the dynamical behavior of $P_z(t)$ remain very similar. However, relaxation processes induced by the same system-bath couplings α are substantially s -dependent and, therefore, differ in all three figures. For example, $P_z(t)$ for $\alpha = 0.01$ and $T = 0.5$ exhibits monotonic decay in Fig. 2 (incoherent regime), shows a single oscillation in Fig. 3 (pseudo-coherent regime), and reveals underdamped evolution in Fig. 4 (coherent regime).

A quick perusal of Figs. 2-4 reveals that transitions between coherent, incoherent and pseudo/quasi coherent regimes are substantially temperature-dependent (see Refs.^{51,52} and references therein for the precise definition of these regimes). However, a comprehensive analysis of the corresponding phase diagrams requires a painstaking characterization of $P_z(t)$ dynamics for the entire set of values of α and s , which is outside the scope of the present work. Interestingly though that increasing temperature decreases periods of Rabi oscillations in the underdamped regime. This is illustrated by Fig. 5, which shows $P_z(t)$ calculated for $s = 0.25$ and $\alpha = 0.01$ at different temperatures. The obtained result is in full agreement with the short-time-inspired effective Rabi formulas (38) and

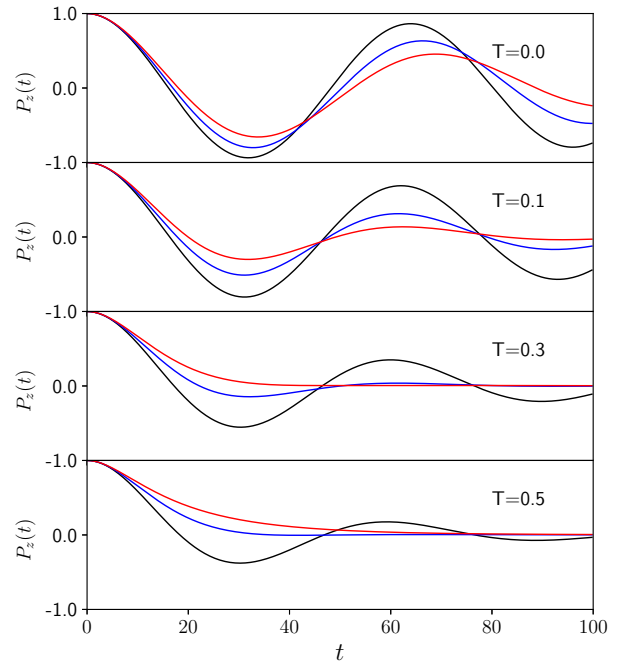


Figure 4. Same as in Fig. 2 but for $s = 0.75$.

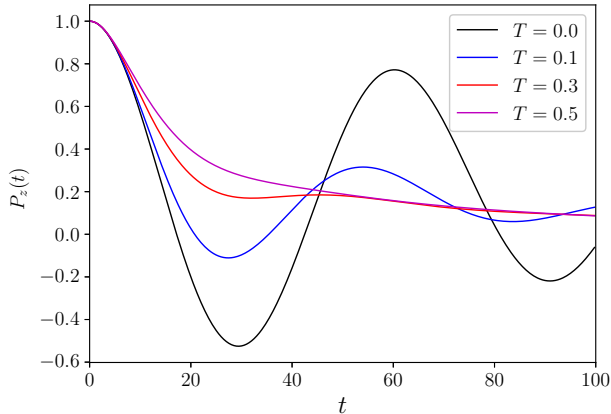


Figure 5. Spin dynamics $P_z(t)$ for the bath with $s = 0.25$ and $\alpha = 0.01$ at different temperatures indicated in the legend.

(39).

To characterize temperature effect in more details, let us consider Fig. 6. Panel (a) shows $P_z(t)$ calculated for $s = 0.25$ and $\alpha = 0.1$ at different temperatures up to $t = 10$. At $t < 1$, $P_z(t)$ is temperature-independent and is solely specified by the Zeno time $\tau_Z = \Delta^{-1}/\sqrt{2}$, in full agreement with Eq. (35). For $1 < t < 4.5$, $P_z(t)$ increase with T which is also fully consistent with the prediction of Eq. (35). Then a cascade of bifurcations occurs: within $4.5 < t < 5.5$ it changes from the lowermost to the uppermost position. The black curve ($T = 0$) swaps the ordering: within $4.5 < t < 5.5$ it changes from the lowermost to the uppermost position. The blue curve ($T = 0.1$) undergoes a similar trend, changing from the second from below to the second from above within $4.5 < t < 7$. The red curve ($T = 0.3$) also changes the ordering, which happens at longer times. This is illustrated by panel (b) which shows the same $P_z(t)$ but calculated up to $t = 100$. Clearly, the red ($T = 0.3$) and magenta ($T = 0.5$) curves swap at $t \approx 40$, so that the order of the curves at $t > 40$ (the curves for the higher temperature are on the bottom) is opposite to that at short times (the curves for the higher temperature are on the top).

The populations $P_z(t)$ evaluated for $s = 0.5$, $\alpha = 0.2$ as depicted in Fig. 7 undergo similar evolutions and transformations, but at slightly different timescales. The curves in Fig. 7(a), similar to their counterparts in Fig. 6(a), are temperature-independent for $t < 1$ and increase with temperature for $1 < t < 6.5$. The black curve ($T = 0$) changes from the lowermost to the uppermost position within $6.5 < t < 10$. The subsequent population dynamics can be followed in Fig. 7(b), which displays the same $P_z(t)$ on the timescale up to $t = 100$. The blue curve ($T = 0.1$) changes from the second from below to the second from above within $6.5 < t < 20$. However, as distinct from Fig. 6, the curves for $T = 0.3$ (red) and $T = 0.5$ (magenta) retain their ordering predicted by the short-time formula (35).

A different scenario is illustrated by Fig. 8 which corresponds to $s = 0.75$ and $\alpha = 0.3$. In this case, the black curve ($T = 0$) changes from the lowermost (as predicted by

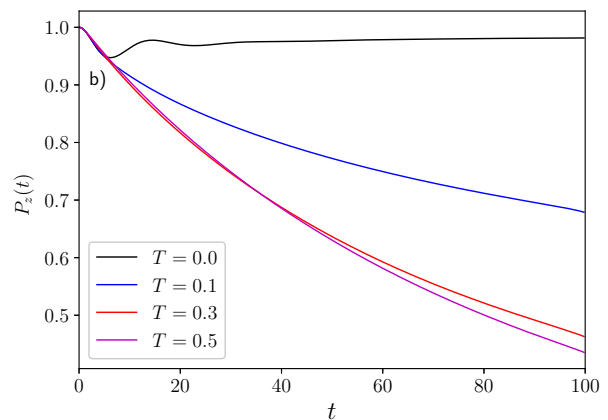
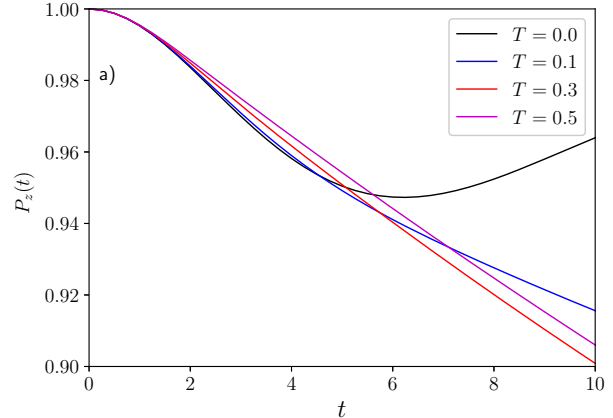


Figure 6. (a) Spin dynamics $P_z(t)$ for the bath with $s = 0.25$ and $\alpha = 0.1$ at different temperatures indicated in the legends. (a) $0 \leq t \leq 10$. (b) $0 \leq t \leq 100$.

the short-time expansion of Eq. (35)) to the uppermost within $0 < t < 28$, while the remaining curves for finite temperatures do not exhibit any change of the order, at least for the time up to $t = 100$.

We thus come up with the following three-stage scenario of $P_z(t)$. The first, temperature-independent stage is specified by the Zeno time τ_Z , which depends solely on the tunneling Δ . The physical origin of this stage is well understood^{89,90} and is determined by the structure of the SBM (or, in a more general case, excitonic) Hamiltonian. The qualitative explanation of this behavior is as follows. The action of the bosonic bath does not show up in the system dynamics instantaneously, and τ_Z is precisely the time required for the system to feel the impact of the bath. The second stage is characterized by the increase of $P_z(t)$ with temperature, which can be attributed to the coupling of the bosonic DOFs to electronic DOFs (polaron effect). Indeed, Eq. (35) can be equivalently rewritten in the form of $P_z(t) \approx 1 - 2\tilde{\Delta}(t, T)^2 t^2$, where the effective tunneling parameter is defined as $\tilde{\Delta}(t, T) = \Delta^2(1 - t^2 \Omega_\mu^2(T))$. Since the Rabi frequency $\Omega_\mu(T)$ increases with T , the effective tunnel-

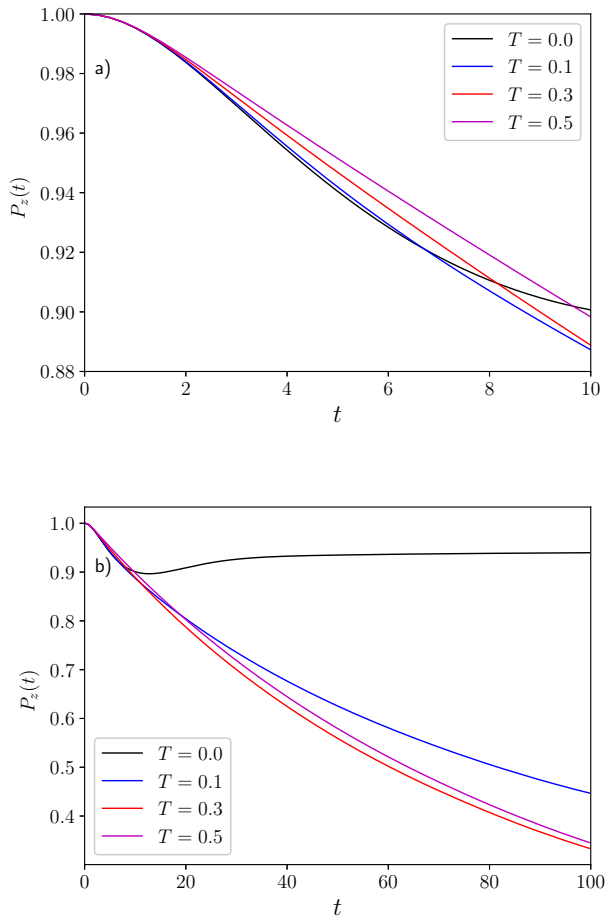


Figure 7. Spin dynamics $P_z(t)$ for the bath with $s = 0.5$ and $\alpha = 0.2$ at different temperatures indicated in the legends. (a) $0 \leq t \leq 10$. (b) $0 \leq t \leq 100$.

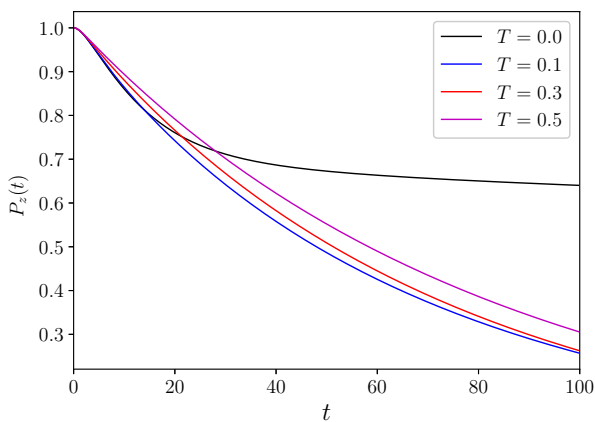


Figure 8. Spin dynamics $P_z(t)$ for the bath with $s = 0.75$ and $\alpha = 0.3$ at different temperatures indicated in the legends.

ing $\bar{\Delta}(t, T)$ decreases with T , owing to the electron-vibrational (polaron) coupling.^{91,92} The third stage, which may or may not occur for specific α , s , and T , is specified by the cascade of bifurcations at which the populations change their short-time ordering. This third stage is therefore characterized by the decrease of $P_z(t)$ with T . Physically, this is a direct consequence of the increasing number of the populated bath states. Since each pair of these states contributes (with a certain weight) to the reduced system dynamics and the transition frequencies between these states are, in general, incommensurable, the summations over the increasing number of these oscillatory-in-time contributions quenches $P_z(t)$. The bifurcation times separating the second and third stages of $P_z(t)$ depend significantly on the bath parameters α and s , as well as on the temperature T . It is unlikely that the bifurcation phenomenon is related to the effective dynamical asymmetry discussed in Ref.⁴⁷ for the SBM with $\varepsilon = 0$, because this asymmetry is not restricted to short times but persists over the entire range of the evolution of the SBM.

IV. CONCLUSIONS

We employed both analytical and numerical tools to comprehensively study finite-temperature dynamics of the sub-Ohmic SBM under shifted (polarized) initial conditions. Several technical milestones have to be highlighted. First, we proved the theorem which maps the dynamics of the SBM governed by the Hamiltonian of \hat{H} under shifted initial conditions onto those governed by the renormalized Hamiltonian of \hat{H}_μ under factorized initial conditions. Second, the theorem facilitated the development of efficient and numerically accurate method for the simulation of dynamics of the SBM under shifted initial conditions. The method is based on the powerful HEOM-TSTT integrator designed for the simulation of multidimensional quantum systems under the factorized initial condition. Third, the theorem was used for the evaluation of first few terms in the Taylor-series expansion of the population $P_z(t)$, which substantially aided the interpretation of the numerics.

The main results of our simulations can be briefly summarized as follows. First, we demonstrated high sensitivity of the dynamics to both initial preparation of the bath and temperature. Second, we gave the benchmark results which could be used for testing other, accurate and approximate, simulation methods and protocols. Third, we discovered the bifurcation phenomenon, which separates two regimes of the dynamics in the time domain. Before the bifurcation time, elevated temperatures slow down $P_z(t)$. After the bifurcation time, they accelerate $P_z(t)$.

We predicted that the established bifurcation phenomenon is general and can be found in other dissipative systems. Furthermore, it is potentially of great interest, because it demonstrates that the initial preparation of the bath (polarized bath + temperature) allows us to efficiently manipulate depopulation rates. Taking into account recent progress in engineering and/or emulation of bosonic baths with arbitrary spectral densities,⁹³⁻⁹⁵ the bifurcation phenomena may open up

exciting perspectives for the optimization and the control of nanosystems.

ACKNOWLEDGMENTS

L. P. Chen acknowledges support from the Key Research Project of Zhejiang Lab (No. 2021PE0AC02). M. F. G. acknowledges support from the National Natural Science Foundation of China (Grant No. 22373028). H. T. and R. B. acknowledge the support by the Spoke 7 "Materials and Molecular Sciences" of ICSC – Centro Nazionale di Ricerca in High-Performance Computing, Big Data and Quantum Computing, funded by European Union – NextGenerationEU.

DATA AVAILABILITY

Further data that support the findings of this study are available from the corresponding author upon reasonable request.

REFERENCES

- ¹A. J. Leggett, S. Chakravarty, A. T. Dorsey, M. P. A. Fisher, A. Garg, and W. Zwerger, *Rev. Mod. Phys.* **59**, 1 (1987).
- ²U. Weiss, *Quantum Dissipative Systems*, 3rd ed. (World Scientific, Singapore, 2007)
- ³H. P. Breuer, F. Petruccione, *The theory of open quantum systems*, Oxford University Press, USA, 2007.
- ⁴L. Chen, P. Shenai, F. Zheng, A. Somoza, and Y. Zhao, *Molecules*. **20**, 15224-15272 (2015).
- ⁵M. F. Gelin, L. Chen, and W. Domcke, *Chem. Rev.* **122**, 17339-17396 (2022).
- ⁶D. E. Makarov, N. Makri, *Chem. Phys. Lett.* **221**, 482-491 (1994).
- ⁷N. Makri, D. E. Makarov, *J. Chem. Phys.* **102**, 4611 (1995).
- ⁸Y. Tanimura, *J. Phys. Soc. Jpn.* **75**, 082001 (2006).
- ⁹Y. Tanimura, *J. Chem. Phys.* **153**, 020901 (2020).
- ¹⁰L. Mühlbacher, J. Ankerhold, C. Escher, *J. Chem. Phys.* **121**, 12696 (2004).
- ¹¹L. Mühlbacher, J. Ankerhold, *J. Chem. Phys.* **122**, 184715 (2005).
- ¹²M. H. Beck, A. Jackle, G. A. Worth, H. D. Meyer, *Phys. Rep.* **324**, 1-105 (2000)
- ¹³H. Wang, M. Thoss, *J. Chem. Phys.* **119**, 1289-1299 (2003).
- ¹⁴H. Wang, M. Thoss, *J. Chem. Phys.* **124**, 034114 (2006).
- ¹⁵U. Manthe, *J. Chem. Phys.* **128**, 164116 (2008).
- ¹⁶M. A. Cazalilla and J. B. Marston, *Phys. Rev. Lett.* **88**, 256403 (2002).
- ¹⁷S. R. White and A. E. Feiguin, *Phys. Rev. Lett.* **93**, 076401 (2004).
- ¹⁸J. Prior, A. W. Chin, S. F. Huelga, and M. B. Plenio, *Phys. Rev. Lett.* **105**, 050404 (2010).
- ¹⁹U. Schollwöck, *Ann. Phys.* **326**, 96 (2011).
- ²⁰G. Vidal, *Phys. Rev. Lett.* **91**, 147902 (2003).
- ²¹G. Vidal, *Phys. Rev. Lett.* **93**, 040502 (2004).
- ²²Y. Zhao, *J. Chem. Phys.* **158**, 080901 (2023).
- ²³Y. Zhao, K. Sun, L. Chen and M. Gelin, *WIREs Comp. Mol. Sci.* **12**, e1589 (2022).
- ²⁴D. V. Shalashilin, *J. Chem. Phys.* **130**, 244101 (2009).
- ²⁵D. V. Shalashilin, *J. Chem. Phys.* **132**, 244111 (2010).
- ²⁶L. Chen, M. F. Gelin, and D. V. Shalashilin, *J. Chem. Phys.* **151**, 244116 (2019).
- ²⁷J. Haegeman, T.J. Osborne, and F. Verstraete. *Phys. Rev. B.* **88**, 075133 (2013).
- ²⁸V. Murg, F. Verstraete, R. Schneider, P. R. Nagy, Ö. Legeza. *J. Chem. Theory. Comput.* **11**, 1027-1036 (2015).
- ²⁹F. A. Y. N. Schröder and A. W. Chin. *Phys. Rev. B.* **93**, 075105 (2016).
- ³⁰B. Kloss, Y. Bar Lev, D. Reichman. *Phys. Rev. B.* **97**, 024307 (2018).
- ³¹P. Sebastian, K. Thomas, S. Andreas. R. M. Salvatore, S. Ulrich, H. Claudius, *Ann. Phys.* **411**, 167998 (2019).
- ³²R. Borrelli, M. F. Gelin, *WIREs. Comput. Mol. Sci.* **11**, e1539 (2021).
- ³³Y. Makhlin, G. Schon, and A. Shnirman, *Rev. Mod. Phys.* **73**, 357 (2001).
- ³⁴D. Vion, A. Aassime, A. Cotter, P. Joyez, H. Pothier, C. Urbina, D. Esteve, and M. H. Devoret, *Science.* **296**, 886 (2002).
- ³⁵A. Shnirman, G. Schön, I. Martin, and Y. Makhlin, *Phys. Rev. Lett.* **94**, 127002 (2005).
- ³⁶X. You, A. A. Clerk, and J. Koch, *Phys. Rev. Res.* **3**, 013045 (2021).
- ³⁷C. Seoanez, F. Guinea, and A. H. Castro Neto, *Europhys. Lett.* **78**, 60002 (2007).
- ³⁸C. Galland, A. Högele, H. E. Türeci, and A. Imamoglu, *Phys. Rev. Lett.* **101**, 067402 (2008).
- ³⁹R. A. Marcus and N. Sutin, *Biochim. Biophys. Acta.* **811**, 265 (1985).
- ⁴⁰L. Mühlbacher and R. Egger, *J. Chem. Phys.* **118**, 179 (2003).
- ⁴¹R. Bulla, N. H. Tong, and M. Vojta, *Phys. Rev. Lett.* **91**, 170601 (2003).
- ⁴²A. Winter, H. Rieger, M. Vojta, and R. Bulla. *Phys. Rev. Lett.* **102**, 030601 (2009).
- ⁴³A. Alvermann and H. Fehske. *Phys. Rev. Lett.* **102**, 150601 (2009).
- ⁴⁴A. Miessen, P. J. Ollitrault, I. Tavernelli, *Phys. Rev. Res.* **3**, 043212 (2021).
- ⁴⁵H. Wang and M. Thoss, *New. J. Phys.* **10**, 115005 (2008).
- ⁴⁶H. Wang and M. Thoss, *Chem. Phys.* **370**, 78 (2010).
- ⁴⁷P. Nalbach and M. Thorwart, *Phys. Rev. B.* **81**, 054308 (2010).
- ⁴⁸F. A. Y. N. Schröder, and A. W. Chin, *Phys. Rev. B.* **93**, 075105 (2016).
- ⁴⁹D. Kast and J. Ankerhold, *Phys. Rev. Lett.* **110**, 010402 (2013).
- ⁵⁰D. Kast and J. Ankerhold, *Phys. Rev. B.* **87**, 134301 (2013).
- ⁵¹F. Otterpohl, P. Nalbach, and M. Thorwart, *Phys. Rev. Lett.* **129**, 120406 (2020).
- ⁵²L. Chen, Y. Y. Yan, M. F. Gelin, and Z. G. Lü, *J. Chem. Phys.* **158**, 104109 (2023)
- ⁵³R. Borrelli, M. F. Gelin, *J. Chem. Phys.* **145**, 224101 (2016).
- ⁵⁴L. Wang, L. Chen, N. Zhou, and Y. Zhao, *J. Chem. Phys.* **144**, 024101 (2016).
- ⁵⁵R. Borrelli. *J. Chem. Phys.* **150**, 234102 (2019).
- ⁵⁶R. Borrelli, and M. F. Gelin. *Sci. Rep.* **7**, 9127 (2017).
- ⁵⁷H. Umezawa, H. Matsumoto, and M. Tachiki, *Thermo Field Dynamics and Condensed States* (North-Holland, Netherlands, 1982).
- ⁵⁸M. Suzuki. *Int. J. Mod. Phys. B.* **10**, 1637-1647 (1996).
- ⁵⁹R. Borrelli, and S. Dolgov. *J. Phys. Chem. B.* **125**, 5397-5407 (2021).
- ⁶⁰Q. Shi, Y. Xu, Y. Yan, and M. Xu. *J. Chem. Phys.* **148**, 174102 (2018).
- ⁶¹R. Kubo. *J. Phys. Soc. Jpn.* **17**, 1100 (1962).
- ⁶²A. Ishizaki, T. R. Calhoun, G. S. Schlau-Cohen, and G. R. Fleming. *Phys. Chem. Chem. Phys.* **12**, 7319-7337 (2010).
- ⁶³J. Hu, M. Luo, F. Jiang, R. X. Xu, and Y. Yan. *J. Chem. Phys.* **134**, 244106 (2011).
- ⁶⁴J. Hu, R. X. Xu, and Y. Yan. *J. Chem. Phys.* **133**, 101106 (2010).
- ⁶⁵M. Xu, Y. Yan, Q. Shi, J. Ankerhold, and J. T. Stockburger. *Phys. Rev. Lett.* **129**, 230601 (2022).
- ⁶⁶Y. Tanimura, and R. Kubo. *J. Phys. Soc. Jpn.* **58**, 101-114 (1989).
- ⁶⁷Q. Shi, L. Chen, G. Nan, R. X. Xu, and Y. Yan. *J. Chem. Phys.* **130**, 084105 (2009).
- ⁶⁸Y. Tanimura, and R. Kubo. *J. Phys. Soc. Jpn.* **58**, 1199-1206 (1989).
- ⁶⁹A. Ishizaki, and Y. Tanimura. *J. Phys. Soc. Jpn.* **74**, 3131-3134 (2005).
- ⁷⁰Y. Ke, R. Borrelli, and M. Thoss. *J. Chem. Phys.* **156**, 194102 (2022).
- ⁷¹Y. Ke, J. Dvořák, M. Čížek, R. Borrelli, and M. Thoss. *J. Chem. Phys.* **159**, 024703 (2023).
- ⁷²I. S. Dunn, R. Tempelaar, and D. R. Reichman. *J. Chem. Phys.* **150**, 184109 (2019).
- ⁷³T. Kramer, M. Noack, A. Reinefeld, M. Rodríguez, and Y. Zelinskyy. *J. Comput. Chem.* **39**, 1779-1794 (2018).
- ⁷⁴C. Lubich, I. V. Oseledets, and B. Vandereycken. *SIAM J. Numer. Anal.* **53**, 917-941 (2015).
- ⁷⁵C. Lubich, and I. V. Oseledets. *Bit Numer Math.* **54**, 171-188 (2014).
- ⁷⁶I. V. Oseledets, and E. E Tyrtshnikov. *SIAM J. Sci. Comput.* **31**, 3744-3759 (2009).
- ⁷⁷I. V. Oseledets. *SIAM J. Sci. Comput.* **33**, 2295-2317 (2011).
- ⁷⁸S. Holtz, T. Rohwedder, and R. Schneider. *Numer. Math.* **120**, 701-731 (2012).
- ⁷⁹P. S. Thomas, and T. Carrington. *J. Phys. Chem. A.* **119**, 13074-13091 (2015).

- ⁸⁰S. Dolgov, B. N. Khoromskij, and I. V. Oseledets. *SIAM J. Sci. Comput.* **34**, A3016-A3038 (2012).
- ⁸¹S. Dolgov and D. Savostyanov. *SIAM J. Sci. Comput.* **36**, A2248-A2271 (2014).
- ⁸²M. Fannes, B. Nachtergaele, and R. F. Werner. *Commun. Math. Phys.* **144**, 443-490 (1992).
- ⁸³D. Perez-Garcia, F. Verstraete, M. M. Wolf, and J. I. Cirac. *Quantum Info. Comput.* **7**, 401-430 (2007).
- ⁸⁴F. Andersson and M. Marcus. *SIAM J. Matrix Anal. Appl.* **39**, 1470-1488 (2018).
- ⁸⁵D. Potts and M. Tasche. *Linear Algebra Appl.* **439**, 1024-1039 (2013).
- ⁸⁶R. Roy and T. Kailath. *IEEE Trans. Acoustics, Speech and Signal Process.* **37**, 984-995 (1989).
- ⁸⁷G. Beylkin and L. Monzón. *Appl Comput Harmon Anal.* **19**, 17-48 (2005).
- ⁸⁸Z. H. Chen, Y. Wang, X. Zheng, R.X. Xu, Y. J. Yan. *J. Chem. Phys.* **156**, 221102 (2022).
- ⁸⁹P. Facchi, S. Pascazio, *Fortschr. Phys.* **49**, 941 (2001).
- ⁹⁰M. F. Gelin, R. Borrelli, W. Domcke, *J. Phys. Chem. Lett.* **10**, 2806 (2019).
- ⁹¹F. A. Pollock, D. P. S. McCutcheon, B. W. Lovett, E. M. Gauger, A. Nazir, *New J. Phys.* **15**, 075018 (2013).
- ⁹²L. Chen, M. F. Gelin, W. Domcke, Y. Zhao, *J. Chem. Phys.* **142**, 164106 (2015).
- ⁹³D. Kienzler, H. Y. Lo, B. Keitch, L. De Clerco, F. Leupold, F. Lindenfesler, M. Marinelli, V. Negnevitsky, J. P. Home, *Science.* **347**, 53-56 (2015).
- ⁹⁴A. Stehli, J. D. Brehm, T. Wolz, A. Schneider, H. Rotzinger, M. Weides, A. V. Ustinov. *npj Quant. Inform.* **9**, 61 (2019).
- ⁹⁵J. M. Kitzman, J. R. Lane, C. Undershute, P. M. Harrington, N. R. Beysengulov, C. A. Mikolas, K. W. Murch, and J. Pollanen, *Nat. Comm.* **14**, 3910 (2023).